

Classification of fold/hom and fold/Hopf spike-adding phenomena

Roberto Barrio,^{1, a)} Santiago Ibáñez,^{2, b)} Lucía Pérez,^{2, c)} and Sergio Serrano^{1, d)}

¹⁾Departamento de Matemática Aplicada and IUMA. Computational Dynamics group. University of Zaragoza. E-50009. Spain.

²⁾Departamento de Matemáticas. University of Oviedo. E-33007 Oviedo. Spain.

(Dated: 1 March 2021)

Hindmarsh-Rose neural model is widely accepted as an important prototype for fold/hom and fold/Hopf burstings. In this paper we are interested in the mechanisms for the production of extra spikes in a burst, and we show the whole parametric panorama in a unified way. In the fold/hom case two types are distinguished, the continuous one, where the bursting periodic orbit goes through bifurcations, but persists along the whole process, and the discontinuous one, where the transition is abrupt and happens after a sequence of chaotic events. In the former case we speak about canard-induced spike-adding and, in the second one, about chaos-induced. For fold/Hopf bursting, a single (and continuous) mechanism is distinguished. **Separately, all these mechanisms are presented, to some extent, in the literature. However, our full perspective allows us to construct a spike-adding map and, more significantly, to understand the dynamics exhibited when borders are crossed, that is, transitions between types of processes, a crucial point not previously studied.**

Keywords: neuron models, fold/hom bursting, fold/Hopf bursting, spike-adding mechanisms

AMS codes: 37B10, 65P20, 92B20

Among the elements that allow communication between neurons, spikes or action potentials are major pieces. **Spike trains (bursts) allow the brain to build a language for the transmission of information since they are signals with a higher probability of being picked up by neighbouring neurons than an isolated spike.**¹ Moreover, the number and the temporal pattern of spikes provide a system for encoding messages. Facing this context, understanding how spikes can be gained (or lost) becomes a central question. This is the goal of this work, taking the Hindmarsh-Rose equations as a paradigm for certain classes of bursting, we analyse three different types of spike-adding processes. Although most of the involved dynamics and bifurcations are well known, we will be able to discover some novel characteristics. Our classification of the different spike-adding mechanisms determines maps in the parameter space that are shown to help in the global analysis of the system. **But, as maps are useless if frontiers are unclear, in this work we deal with the dynamics that characterize the transitions from one to another type of spike-adding. Moreover, some common elements necessary in our discussion are also present in neural and other problems (mechanics, chemistry, ...), such as the existence in numerical and experimental studies of comb-shaped chaotic regions and the spike-adding phenomenon²⁻⁵, so this work can help in the exploration of these systems. Challenges in neuroscience and, in particular, the problems that still remain to be solved in deciphering the language of neurons are impressive. Undoubtedly, the classification of the different mechanisms involved in the genesis of extra action potentials is an essential element of that big task.**

I. INTRODUCTION

Bursting is one of the most relevant phenomena that can be observed in a neuron. Roughly speaking, bursting is characterized by the appearance of sequences of spikes, corresponding to fast discharges, alternating with periods of quiescence. Moreover, when dealing with a bursting neuron, one of the major challenges is to understand how spikes are added to a given train of signals.

This paper studies the spike-adding mechanisms exhibited in the Hindmarsh-Rose⁶ neuron model, a well known example and prototype of fold/hom (or square-wave) and fold/Hopf bursting^{7,8}. It is able to reproduce the most significant behaviors: quiescence, spiking and also bursting, either regular or irregular (chaotic). Literature concerning this model is extensive and, only in relation to our interests, we can quote Refs. 2, 9–21.

The Hindmarsh-Rose (HR) model is described by the following set of equations:

$$\begin{cases} \dot{x} = y - ax^3 + bx^2 - z + I, \\ \dot{y} = c - dx^2 - y, \\ \dot{z} = \varepsilon[s(x - x_0) - z]. \end{cases} \quad (1)$$

Variable x represents the membrane potential, whereas y and z correspond to ionic currents. We consider a typical choice of parameters with $a = 1$, $c = 1$, $d = 5$ and $s = 4$, discussing the spike-adding processes for different choices of the other b , I and ε .²¹ We assume that ε is a small parameter in the model, giving rise to a fast-slow system with two fast (x and y), and one slow (z) variables.

When $\varepsilon = 0$ in model (1), we obtain a reduced system which is usually called the fast subsystem. Note that the fast subsystem is a family of planar vector fields where z is an additional parameter. Fixing b and I (still with $\varepsilon = 0$), we obtain a bifurcation diagram with respect to z that is illustrated in Fig. 1. There is a curve formed by equilibria which is named the slow manifold (\mathcal{M}_{slow}) and a surface containing limit cy-

^{a)}Electronic mail: rbarrio@unizar.es

^{b)}Electronic mail: mesa@uniovi.es

^{c)}Electronic mail: perezplucia@uniovi.es

^{d)}Electronic mail: sserrano@unizar.es

This is the author's peer reviewed, accepted manuscript. However, the online version of record will be different from this version once it has been copyedited and typeset.
PLEASE CITE THIS ARTICLE AS DOI: 10.1063/5.0037942

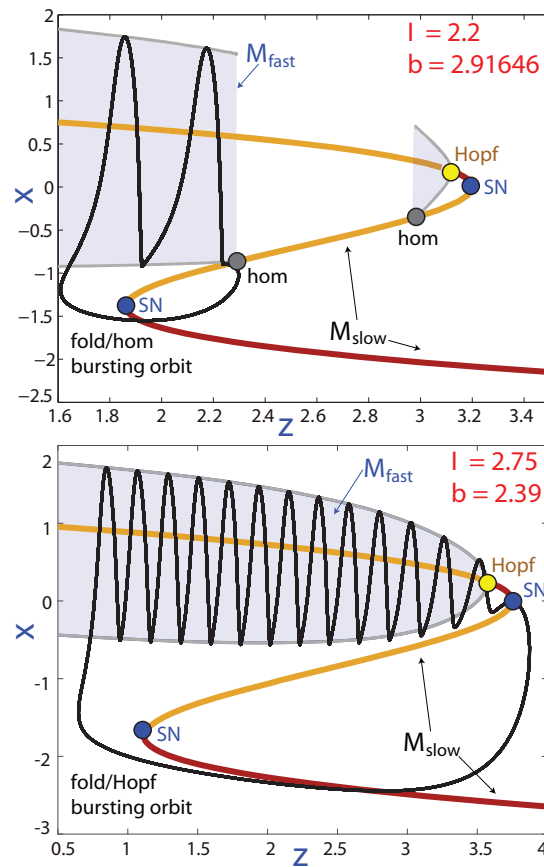


FIG. 1. 2D projection of fold/hom (top) and fold/Hopf (bottom) bursting orbits ($\varepsilon = 0.01$) superimposed (in black) over the classical slow-fast decomposition ($\varepsilon = 0$) of the HR model (1) formed by the 1D slow manifold of stable (dark red) and unstable (orange) equilibria (\mathcal{M}_{slow}) and the 2D fast (spiking) manifold (\mathcal{M}_{fast}) of limit cycles of the fast subsystem of the model (in gray). SN stands for saddle-node bifurcations of equilibria, Hopf denotes the Hopf bifurcation points and hom the homoclinic bifurcation points.

cles which is said the fast manifold (\mathcal{M}_{fast}). Recall that, in a general setting, slow-fast decompositions were first described in Ref. 7. For $I = 2.2$, $b = 2.91646$ (top) and for $I = 2.75$ and $b = 2.39$ (bottom), the slow manifold is shown in dark red (resp. orange) for stable (resp. unstable) equilibria and the fast manifold is shown in gray. Intuitively, one can understand how burst patterns emerge. Fig. 1 also shows stable periodic orbits of the full system (black) superimposed to the bifurcation diagram of the fast subsystem. The slow dynamics in the complete model is such that $\dot{z} < 0$ when fast variables are moving close to the lower branch of \mathcal{M}_{slow} , whereas $\dot{z} > 0$ when they are close to \mathcal{M}_{fast} .

Indeed, as singular perturbation theory and Fenichel's theorems explain²², orbits (for small enough ε) follow both manifolds on some parts of their trajectory. Following the terminology in Ref. 8, in the first case (top panel), the bursting orbit is said to be of fold/homoclinic type, because the termination of the fast subregime is due to the existence of a homoclinic bifurcation in the phase space of the fast subsystem. In the second case (bottom panel), the bursting orbit is said to be of

fold/Hopf type because the amplitude of oscillations during the bursting is decreasing as the limit cycles of the reduced model approach the Hopf bifurcation.

As already mentioned, the main goal of this paper is to explain the processes (spike-adding) that lead a bursting orbit to change its number of spikes per period. More precisely, we provide a classification of the different types of spike-adding processes in fold/hom and fold/Hopf bursters. From Terman²³, in the general context of fold/hom bursting, two spike-adding mechanisms are considered. On the one hand, there can arise extra excursions around the fast manifold which are generated through a discontinuous process linked to a chaotic phenomenon. On the other, there also can happen that extra excursions are created through a continuous process linked to orbits that transit through phase space following the unstable branch of the slow manifold. We will refer to the first scenario as chaos-induced spike-adding, and the second one as canard-induced spike-adding. Both cases have been recently studied in the literature^{9,11,17,19,24}. Note that analytical results have only been obtained very recently on simpler models, such as the in-depth theoretical study on the spike-adding canard transition given by P. Carter in Ref. 25, where the Morris-Lecar model²⁶ is considered (see also Ref. 27 where a transition from 1 to 2 spikes via canard orbits is thoroughly analysed in a different fast-slow system based on the FitzHugh-Nagumo equations). These two interesting papers are the first analytical studies regarding the complete creation of canard orbits in neural models and open an exciting research line. However, it should be noted that the whole scenario is beyond the current analytical techniques.

The spike-adding mechanism in the case of fold/Hopf bursting is completely different and is related to the distance between saddle-node (left SN bifurcation point of Fig. 1(bottom)) and Hopf bifurcation points in the fast subsystem (see Fig. 1). Namely, the number of spikes depends on the length of the oscillation tube which is accessible for orbits after they jump to the fast manifold from the slow manifold. It also depends on the characteristic rotation speed at the Hopf bifurcation point. We will refer to this mechanism for spike-adding as Hopf-induced. Discussions in the literature about the spike-adding mechanism involved in the fold/Hopf bursters are not so common as those about fold/hom scenarios. Of course, in all cases, the number of spikes also increases as ε decreases, but this is not our interest, so we will consider fixed small values of ε .

We will see how the Hindmarsh-Rose model exhibits the three spike-adding mechanisms that we have just described. As said, all have already been considered, to a greater or a lesser extent, in the literature. However, in this paper the treatment is unified, which allows to understand the differences between them. Besides, we pay special attention to the transition dynamics between scenarios, a problem not well studied in literature. Bearing in mind that different spike-adding processes are feasible in a model (HR model in our case), the question is: where and why are they produced?

The frontier between the two spike-adding mechanisms linked to fold/hom bursters will be shown to be sharp. Namely, it will be marked by homoclinic surfaces in the

This is the author's peer reviewed, accepted manuscript. However, the online version of record will be different from this version once it has been copyedited and typeset. PLEASE CITE THIS ARTICLE AS DOI: 10.1063/5.0037942

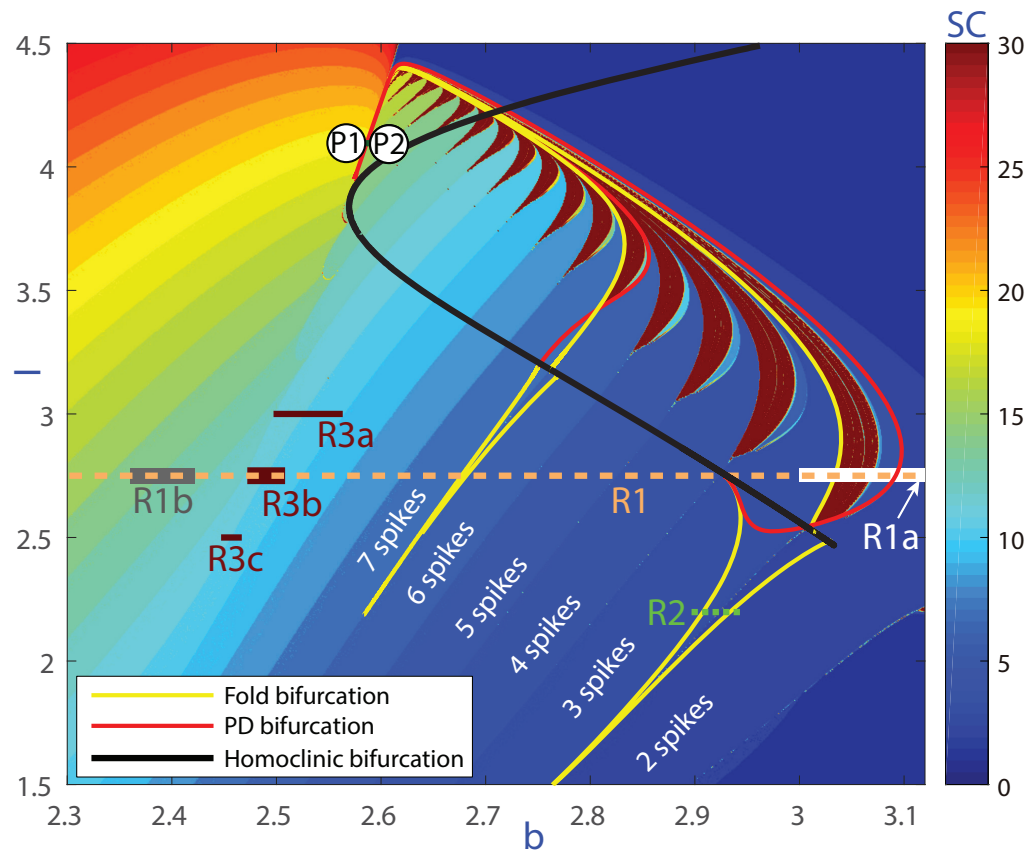


FIG. 2. Biparametric spike-counting bifurcation diagram for $\varepsilon = 0.01$. Different segments are selected to illustrate (on later figures) three different spike-adding processes: chaos-induced discontinuous spike-adding, canard-induced continuous spike-adding and Hopf-induced continuous spike-adding. Along the long segment $R1$ all of them appear; a discontinuous chaos-induced transition from 2 to 3 spikes along segment $R1a$; a continuous Hopf-induced transition from 13 to 14 spikes along segment $R1b$; and continuous canard-induced along segment $R2$ showing a transition from 2 to 3 spikes between fold/hom bursters. Transitions from $P1$ to $P2$ and along the segments $R3a$, $R3b$ and $R3c$ will be described in Section III to explain how dynamics evolve to change from one scenario to another.

111 three-parameter bifurcation diagram.¹⁰ Nevertheless, the sep-133
 112 aration between Hopf-induced processes and either chaos-134
 113 induced or canard-induced will appear fuzzy. Coming from h-35
 114 the region of chaos-induced spike-adding, a fan of bifurca-136
 115 tions must be crossed to enter into the region corresponding-37
 116 to Hopf-induced processes. These bifurcations arise from a-38
 117 codimension-two homoclinic bifurcation point. As we will
 118 recall later, in the case of a canard-induced spike-adding, the
 119 periodic orbit must undergo several periodic orbit bifurca-139
 120 tions (bistability and hysteresis are present), among them two
 121 curves of fold bifurcations which disappear at cusp²⁸ bifurca-140
 122 tion points. These codimension-two bifurcation points will-141
 123 play the role of boundary stones separating the canard do-142
 124 mains from the Hopf ones. In other words, continuous spike-143
 125 adding can be canard-induced or Hopf-induced. The first case-144
 126 happens when the continuation of the periodic orbit includes-145
 127 paths of unstable regime. When this course is not realizable-146
 128 because no bifurcation is accessible (the continuation curve is-147
 129 far from the cusp boundary stones), the gaining of extra spikes-148
 130 can be explained through a Hopf bifurcation process. 149

131 All the different types of spike-adding mechanisms are de-150
 132 tailed in Section II, showing how they indeed arise in the-151

Hindmarsh-Rose model. Transitions between these mecha-
 nisms will be described in Section III. Results are summarized
 and discussed in Section IV, where a theoretical classification
 parametric map is proposed. Conclusions are provided in Sec-
 tion V. Throughout this article, all the continuation analysis
 has been done using the well known software AUTO^{29,30}.

II. CLASSIFICATION OF SPIKE-ADDING PHENOMENA

In this section we describe the different spike-adding phe-
 nomena present in the HR model. On Fig. 2, regions with
 periodic attractors with a different number of spikes are rep-
 resented in different colors (spike-counting technique). From
 dark blue, indicating spiking, towards red, the number of
 spikes of the periodic orbit grows. Dark red indicates that
 the maximum number of spikes considered in the method has
 been exceeded, meaning that in a large part of that region
 the dominant behavior is chaotic².

This figure shows a typical situation for small ε values (in
 this case $\varepsilon = 0.01$). There exist a finite collection of homo-
 clinic bifurcation curves, the black curve represented in the

This is the author's peer reviewed, accepted manuscript. However, the online version of record will be different from this version once it has been copyedited and typeset.
PLEASE CITE THIS ARTICLE AS DOI: 10.1063/1.50037942

152 figure being one of them. All the others are so close that, if
153 they were also depicted, they would overlap with each other
154 (see details in Ref. 10). Located on such curves there also
155 arise codimension-two homoclinic bifurcations from which
156 many of the elements involved in the spike-adding processes
157 emerge. As an illustration, Fig. 2 includes some codimension-
158 one bifurcations of periodic orbits: fold (yellow) and period-
159 doubling (red) curves. Below the homoclinic bifurcation
160 curve, there are wedges corresponding to bistability regimes.
161 These regions are bounded by a pair of fold bifurcations con-
162 necting through a cusp point. Above the homoclinic bifurca-
163 tion curve, lobes of chaotic dynamics are formed contain-
164 ing pencils of period-doubling cascades. These lobes are lim-
165 ited by a fold bifurcation curve of periodic orbits and the first
166 period-doubling cascade.

167 Segment $R1$ in Fig. 2 crosses regions of the biparametric
168 plane showing the three types of spike-adding detected
169 in the model. Along segment $R1a$ we will describe the
170 chaos-induced discontinuous spike-adding (Subsection II A)
171 and segment $R1b$ is selected to explain the Hopf-induced
172 continuous spike-adding (Subsection II C). On the other
173 hand, although canard-induced continuous spike-adding is
174 also present along $R1$, segment $R2$ from Fig. 2 is selected for
175 the purpose of illustration, because it provides a clearer dis-
176 play (Subsection II B).

177 A. Chaos-induced discontinuous spike-adding

178 The first type of spike-adding process that we are going to
179 analyze is the chaos-induced discontinuous one. As we have
180 already mentioned, this process occurs in the region above the
181 homoclinic curve, this curve being a boundary of such region.
182 In Fig. 3 we consider segment $R1a$ of Fig. 2 and we zoom in on
183 the surrounding region with the spike counting technique. Be-
184 low that picture, we show the interspike-interval bifurcation
185 diagram (IBD) of this segment and the $\|\cdot\|_2$ norm of the peri-
186 odic orbits obtained with continuation techniques (AUTO).

187 As we can see in the figure, to the right of the segment there
188 is a bursting periodic attractor with 2 spikes. As b decreases,
189 a typical scenario is present. Firstly, the periodic attractor
190 undergoes a cascade of period-doubling bifurcations, until a
191 chaotic attractor is generated. Within the chaotic region, nar-
192 row windows of regular behavior appear where new periodic
193 orbits are generated. They will go through new bifurcations
194 where they will become unstable joining to the chaotic invari-
195 ant set. Finally, at a fold bifurcation, the chaotic invariant set
196 stop being an attractor and two periodic orbits (one stable and
197 one unstable) with 3 spikes are generated. 209

198 To show how the attractors evolve throughout this spike-
199 adding phenomenon, in Fig. 4 we present the complete pro-
200 cess. The central picture shows the bifurcation diagram ob-
201 tained by continuation (AUTO) corresponding to the segment
202 $R1a$ in Fig. 2. We have selected several values of b (marked
203 in the central picture with small colored squares and num-
204 bers) for which we have plotted these orbits. For these values
205 the periodic orbits (solid line for stable, and dashed for unsta-
206 ble ones) and a chaotic attractor (for square $-6-$) are shown

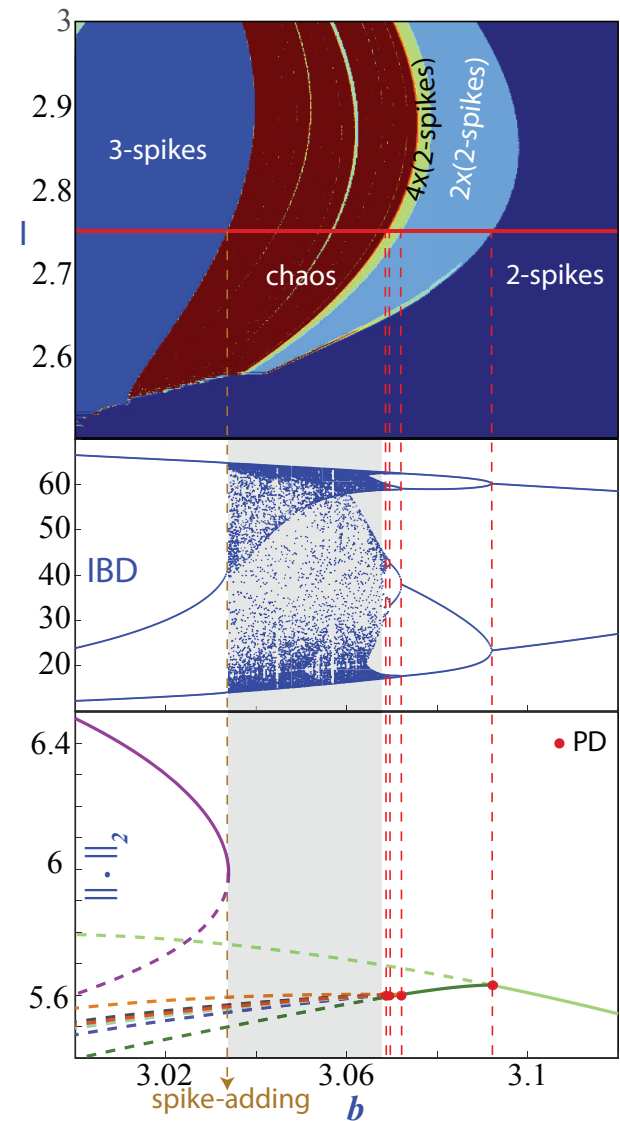


FIG. 3. Analysis of segment $R1a$ (in Fig. 2) with $\varepsilon = 0.01$, $I = 2.75$ and b as bifurcation parameter. Top: Biparametric bifurcation spike-counting diagram around the segment $R1a$. Dark red represents chaos, different colors represent periodic orbits with different bursting. Middle picture shows the IBD bifurcation diagram and the bottom one displays a continuation of the periodic orbits, with different solid (dashed) colors for different (un)stable orbits.

around the central picture. Orbit $-1-$ represents the basic periodic orbit of 2 spikes. After the first period-doubling bifurcation, the orbit $-1-$ becomes unstable and a stable periodic orbit $-2-$ with two bursts with 2 spikes (2×2 orbit) is generated. A second period-doubling bifurcation repeats the former mechanism from 2×2 to 4×2 orbit $-3-$. So, the same mechanism is developed again and again (to a 8×2 orbit $-4-$, 16×2 orbit $-5-$, and so on), a countably infinite number of times giving place to a typical period-doubling route to chaos that generates a chaotic attractor ($-6-$). After a fold bifurcation, the chaotic set becomes unstable and two periodic orbits ($-7-$) with 3 spikes are born (the spike-adding). One

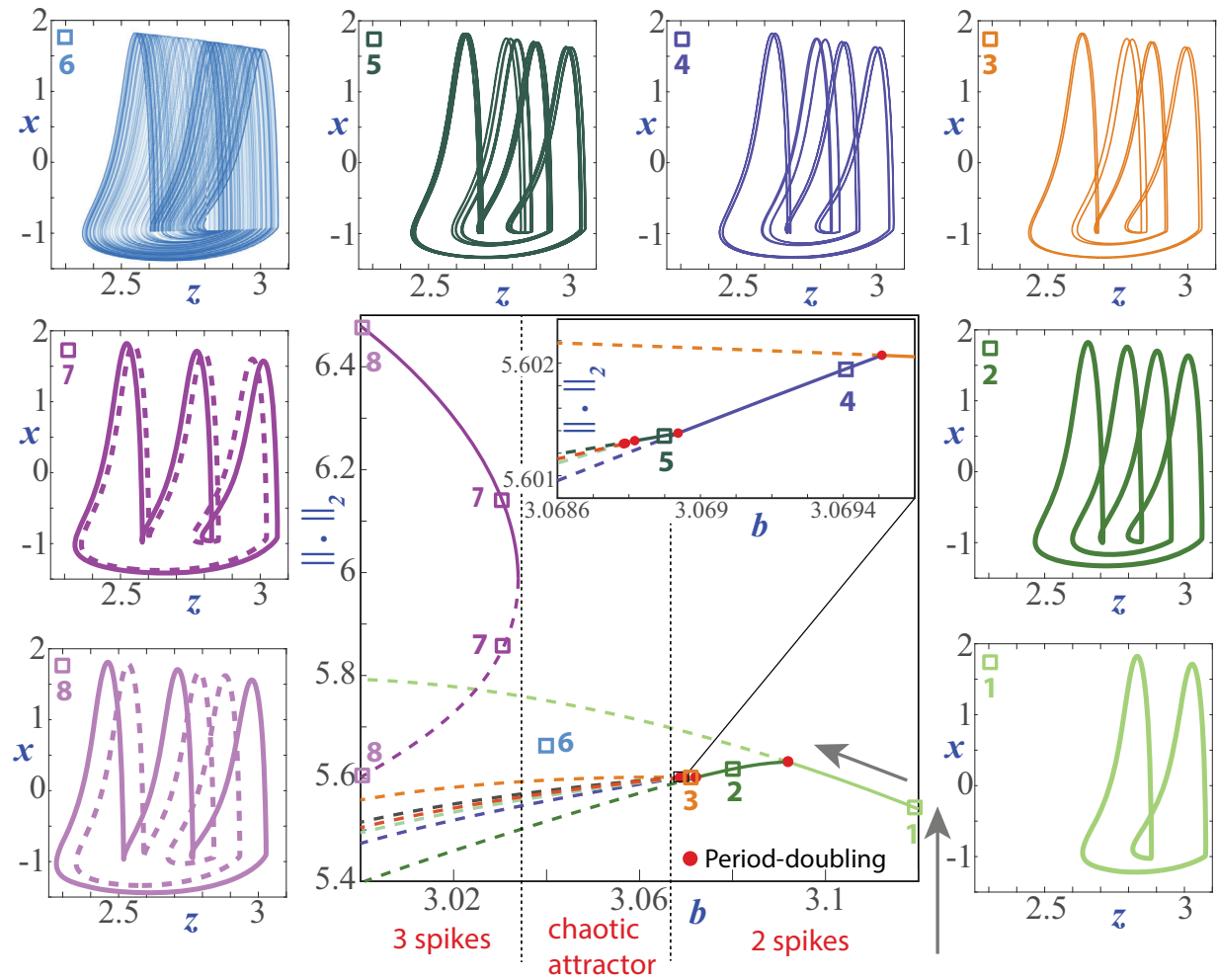


FIG. 4. Evolution of periodic orbits throughout the process of chaos-induced discontinuous spike-adding. Central picture shows the bifurcation diagram obtained by continuation corresponding to the segment $R1a$ in Fig. 2. The coloured squares mark the points in the diagram corresponding to the selected values. For these values, the periodic orbits (solid line for stable, and dashed for unstable ones) and a chaotic attractor (for square $-6-$) are shown around the central picture. Along the continuation of the bifurcation lines we observe periodic orbits with two spikes ($-1-$), later a period-doubling cascade ($-2-$ to $-5-$) originates a chaotic attractor ($-6-$) and, finally, after a fold bifurcation, two periodic orbits with three spikes appear ($-7-$ and $-8-$). In the upper right corner of the central picture, a magnification of the region where the first period-doubling cascade occurs is shown.

219 of them is stable, the other one unstable, both are indistin-235
 220 guishable at the fold bifurcation and they run along the outer-236
 221 edge of the chaotic set. When b moves away from the valu-237
 222 at which the bifurcation occurs, both orbits are separated from-238
 223 each other. 239

240
 241 It is worth paying attention to certain qualitative aspects, 241
 242 that can be observed in the chaotic transition illustrated in, 242
 243 Figure 4. As the attracting periodic orbits that arise through, 243
 244 period-doublings build the chaotic attractor ($-6-$), spikes ar- 244
 245 range visually in four groups inside phase space, although two 244
 246 of them, those placed in central positions, seem to compete to 245
 247 fill the same area. This process is typical in period-doubling 246
 248 cascades giving rise first to thin Feigenbaum chaotic attrac- 247
 249 tors that later merge in thicker and larger ones via boundary 248
 250 crisis phenomena. When the chaotic attractor is fully created, 249
 we clearly see how the groups of spikes give rise to three, not 250

to four, areas within the attractor, characterized by a denser 235
 flow. When the fold bifurcation occurs, the three-spiked sta- 236
 ble periodic orbit takes the place of the chaotic attractor, flow- 237
 ing through the denser areas previously swept by the chaotic 238
 trajectory. The fold bifurcation marks the beginning of a peri- 239
 odic window: the chaotic attractor becomes an unstable sad- 240
 dle chaotic invariant set that embeds, among other unstable 241
 periodic orbits, the unstable orbit itself that is born at the fold 242
 bifurcation. 243

As already pointed out in Ref. 12, the process we have just 244
 described is known in the literature as Type I intermittency 245
 transition to chaos, as introduced in Refs. 31 and 32. In Ref. 246
 12, authors explore a segment of parameters which cuts the 247
 whole sequence of chaotic lobes. The scenario here presented 248
 is common to each spike-adding. As b decreases, periodic or- 249
 bits with n spikes go through a period-doubling cascade which 250

This is the author's peer reviewed, accepted manuscript. However, the online version of record will be different from this version once it has been copyedited and typeset.
PLEASE CITE THIS ARTICLE AS DOI: 10.1063/1.50037942

251 precedes the formation of a horseshoe. The dynamics enters
252 into a chaotic window which disappears through a Type I in-
253 termittency transition. Chaotic transitions have been studied
254 in Refs. 23 and 33. Working in a general framework, which
255 includes the Hindmarsh-Rose model, Terman explains how
256 the passage from n to $n + 1$ spikes can be accompanied by the
257 creation of horseshoes. In that sense, we understood that each
258 passage through a chaotic lobe includes a Terman's transition.

259 B. Canard-induced continuous spike-adding

260 A full detailed picture of the continuous transition from 2
261 to 3 spikes between fold/hom bursters along the segment $R2$
262 (Fig. 2) is given in Fig. 5. In the central panel, the bifurca-
263 tion curve obtained by continuation is displayed. Solid curve
264 represents stable periodic orbits, while dashed curve indicates
265 unstable periodic orbits. Squares with different colors over the
266 curve mark different values of parameter b selected to show
267 their corresponding periodic orbits (pictures around). These
268 periodic orbits are plotted over the slow \mathcal{M}_{slow} and fast \mathcal{M}_{fast}
269 manifolds of the limit case to explain the canard transition
270 generating the new spike^{11,13,17}. In the upper left corner of the
271 central picture, all the selected orbits are represented together
272 to see their relative position. Starting from the lower branch of
273 the bifurcation curve, where the 2-spikes periodic orbit is sta-
274 ble, and decreasing the value of b , the curve reaches a fold bi-
275 furcation (marked with a square inside a circle). There, the pe-
276 riodic orbit becomes unstable and its length starts to increase
277 as b decreases. This is the beginning of the canard transition
278 The increment in the length of the periodic orbit occurs as it
279 extends following the piece of the slow manifold close to the
280 unstable part of the manifold of equilibria between both fold
281 bifurcations (see Fig. 1 top). Along the middle branch of the
282 bifurcation curve, "headless" canards evolve up to a second
283 fold bifurcation is reached. There, the orbit overcomes the
284 right-fold of the equilibrium manifold in the fast subsystem
285 and an additional turn around the tubular fast manifold arises
286 the canard orbit is said maximal and the canard "head" starts
287 to be developed (second fold bifurcation marked with a square
288 in a circle). This "head" moves to the left as b increases and
289 the orbit recovers its stability after a period-doubling bifur-
290 cation (marked with a square inside a circle), when the orbit
291 already has an extra spike. Therefore, the new spike has trav-
292 elled from the neighbourhood of the right piece of \mathcal{M}_{fast} to
293 the neighbourhood of the left piece of \mathcal{M}_{fast} . This process
294 that we have just described is the essential mechanism behind
295 the continuous spike-adding for fold/hom bursters^{11,13,17}.

296 In the sense in which we have travelled the curve, the bifur-
297 cation where the orbit with three spikes regains its stability is
298 actually a period-halving bifurcation. Keep in mind that in
299 small interval to the right of this bifurcation there are pencils
300 of bifurcations very close each other, and so it is quite diffi-
301 cult to observe them and their effects. Just to show this, the
302 doubled periodic orbit emerging at that point is also continued
303 with AUTO and both bifurcation curves are displayed in Fig. 6
304 (light blue color lines). The curve for the double period orbit
305 undergoes through a fold bifurcation where parameter b starts

to increase until a second period-doubling is reached, and so
on (note that the unstable orbit is connected with bifurcated
orbits close to the fold on the right). This process only can
be detected using continuation techniques because the stable
region is very small and it has no real effects in the dynam-
ics. However, once the phenomenon is detected, the orbits
obtained can be carefully integrated to observe the chaotic be-
havior in that narrow parametric region (see red dots on the
IBD on the top picture of Fig. 6).

This canard-induced spike-adding mechanism had already
been discussed in the literature.^{11,13,17,19} Some micro-chaos
zones had already been detected and discussed in Ref. 12,
but for segments very close to the homoclinic bifurcation
curves, and not on the generic spike-adding process. Here
we observe how small chaotic windows are detected far
from the homoclinic skeleton. It follows that the fan of
bifurcations of periodic orbits extends widely in parameter
space. In fact, the chaotic window is associated with a cas-
cade of period-doubling. The tangled bifurcation diagram
formed by the codimension one bifurcations that arise from
the codimension-two homoclinic bifurcation points has been
discussed in Ref. 10, where it is also explained how the spike-
adding mechanisms fit into the whole web.

C. Hopf-induced continuous spike-adding

The Hindmarsh-Rose model presents a variation of con-
tinuous spike-adding, where bistability and canards are not
present. The spike-adding occurs without the periodic orbits
losing their stability, but still increasing their length by adding
an extra cycle to their turns around the fast manifold.

Unlike what happens in the fold/hom cases, in the pro-
cess of Hopf-induced spike-adding, period-doubling and fold
bifurcations do not appear. Neither is chaotic behavior ob-
served, nor do canards emerge. The complete process is
shown in Fig. 7, presenting again in the central panel the con-
tinuation bifurcation diagram of segment $R1b$ of Fig. 2. The
coloured squares mark the points in the diagram correspond-
ing to the selected values. For these values, the stable pe-
riodic orbits are shown over the slow \mathcal{M}_{slow} and fast \mathcal{M}_{fast}
manifolds (see Fig. 1 for more details). As shown in Fig. 7,
the process is straightforward. That is, what happens in this
case is that, as b decreases, almost the entire orbit is moving
toward smaller values of z . But the point of re-entry of the
orbit around the fast manifold, after passing through the sta-
ble lower branch of the slow manifold, does not move. This
means that more space is generated in the corner of the slow
manifold where the upper saddle-node is located. Thus, there
comes a time when there is room for a new spike in the orbit,
which is occupied. As b continues to decrease, the displace-
ment of most of the orbit continues, causing the amplitude of
the new spike to increase. Along the continuation of the bifur-
cation line we observe how periodic orbits with thirteen spikes
move to the left so that space is generated for the appearance
of a new spike on the right side of the orbit giving rise to a
burster with fourteen spikes instead of thirteen. If b contin-
ues to decrease sufficiently, this spike-adding process will be

This is the author's peer reviewed, accepted manuscript. However, the online version of record will be different from this version once it has been copyedited and typeset.
PLEASE CITE THIS ARTICLE AS DOI: 10.1063/1.50037942

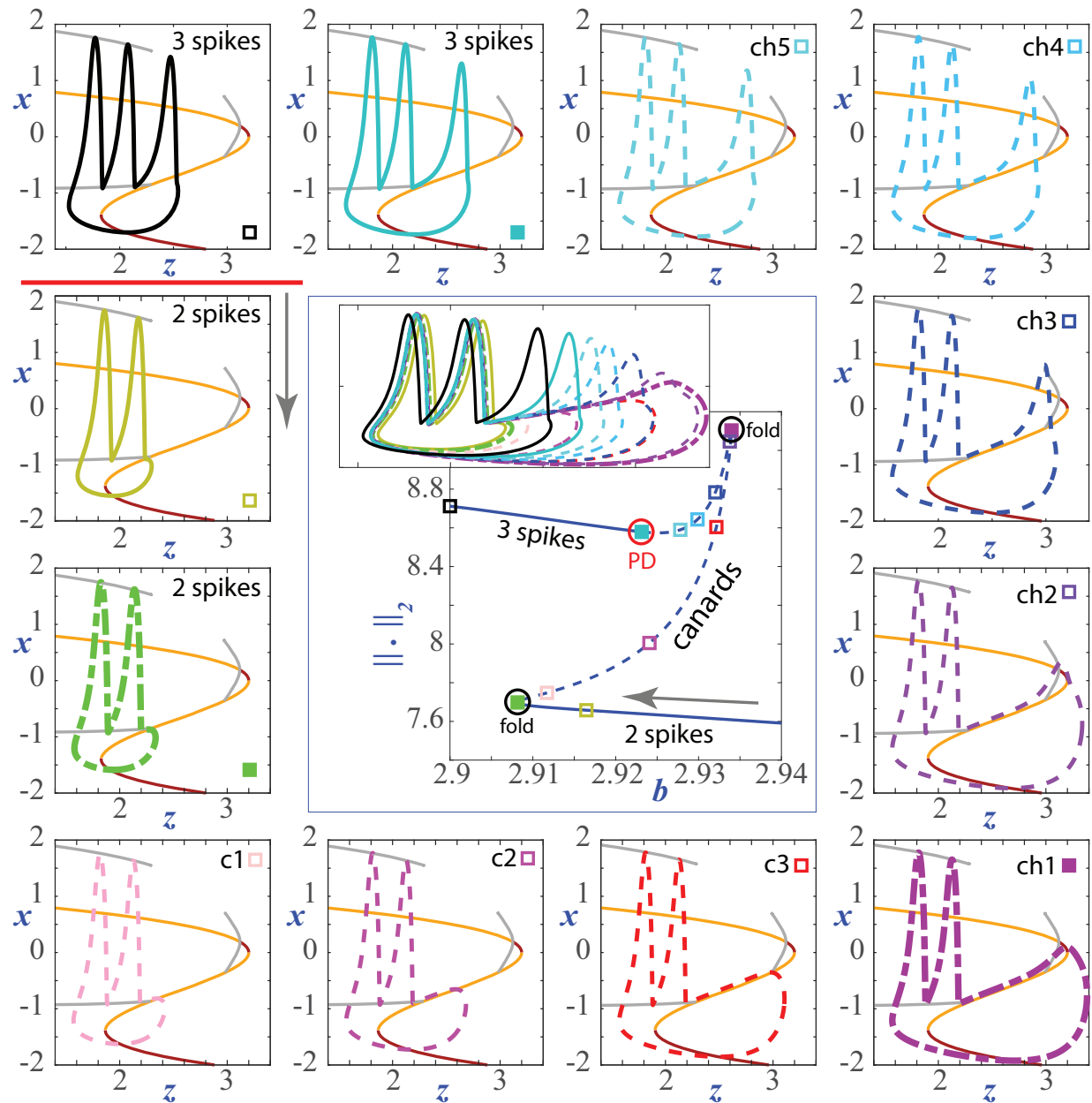


FIG. 5. Evolution of periodic orbits throughout the process of canard-induced continuous spike-adding. Central picture shows the bifurcation diagram obtained by continuation (AUTO) corresponding to the segment $R2$ in Fig. 2. The coloured squares mark the points in the diagram corresponding to the selected values. For these values, the periodic orbits (solid line for stable, and dashed for unstable ones) are shown over the slow and fast manifolds (\mathcal{M}_{slow} and \mathcal{M}_{fast} , see Fig. 1 for more details). The grey arrow indicates the direction in the process of adding a new spike. In the upper left corner of the central picture, all the selected orbits are represented together to see their relative position. Along the continuation of the bifurcation line we observe periodic orbits with two spikes, later headless canards (orbits numbered with -c-), canards with head (-ch- orbits), and, finally, orbits with three spikes.

361 repeated in the same way.

362 As already mentioned in the introduction, any process of
363 spike-adding where periodic orbits do not cross any bifurca-
364 tion, just a smooth change allowing an extra spike, will be
365 referred as Hopf-induced, even in the case where the fast dy-
366 namics does not correspond to a fold/Hopf bursting from the
367 Izhikevich classification.

368 In the Appendix we explain theoretically, using a simple

369 model, how the number of spikes depends on the distance be-
370 tween the two saddle-node bifurcation points of the slow man-
371 ifold of equilibria \mathcal{M}_{slow} . In the case of a fold/Hopf burster,
372 the number of spikes exhibited by an orbit is strongly linked to
373 the size of the oscillation region in the phase space. The trajec-
374 tory around the fast manifold is longer as greater is the width
375 of that region in the direction of variable z and that width cor-
376 responds to the distance between the saddle-node bifurcation

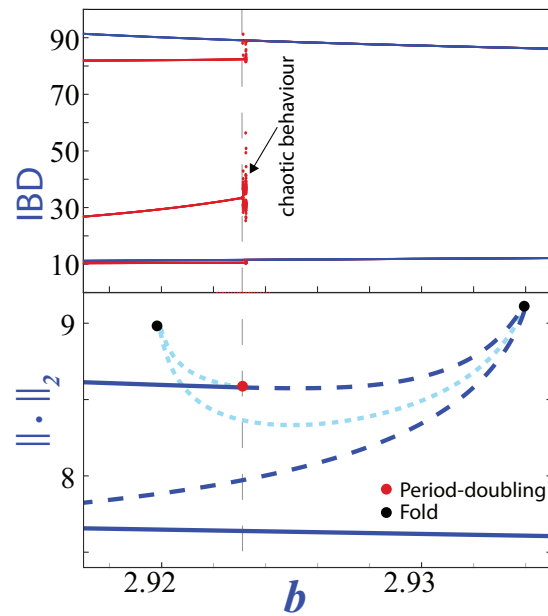


FIG. 6. IBD (top) and continuation diagram (bottom) of a magnification of segment $R2$. On the top picture, blue represents periodic orbits with two spikes while red line represents periodic orbits with three spikes and some bifurcated orbits from them coexisting with the two spikes periodic orbits. In the pointed thin region there exists chaotic behavior (dotted red points) originated via a very narrow period-doubling cascade.

377 points, at least for small values of ε . As b decreases, that dis-
 378 tance increases. To be precise, observe how the lower saddle-
 379 node point moves to left as b decreases, but the upper one
 380 seems to remain fixed.

381 III. TRANSITION SPIKE-ADDING STATES

382 In the previous section we have identified three differ-
 383 ent spike-adding processes, namely, mechanisms induced by
 384 chaotic behaviors, canard explosions or Hopf bifurcations.
 385 Recall that the former is a discontinuous evolution, whereas
 386 the latter two are continuous transitions. Now we explain how
 387 the dynamics is transformed to change from one type to an-
 388 other.

389 We begin by discussing the transition between the two types
 390 of continuous spike-adding. In this case we cannot visually
 391 identify a sharp border marking the passage from one to the
 392 other. Fig. 8 shows the spike-adding process from bursting per-
 393 iodic orbits with 10 spikes to periodic orbits with 11 spikes
 394 along the three small segments $R3a$, $R3b$ and $R3c$ (see Fig.
 395 2). Along the first segment, the process clearly corresponds
 396 to canard-induced continuous spike-adding. In the case of the
 397 third segment, however, the process clearly is Hopf-induced
 398 continuous spike-adding. It is evident that, between these two
 399 segments, a bifurcation has to occur that generates the change
 400 of ε we are not able to detect it numerically as the continu-
 401

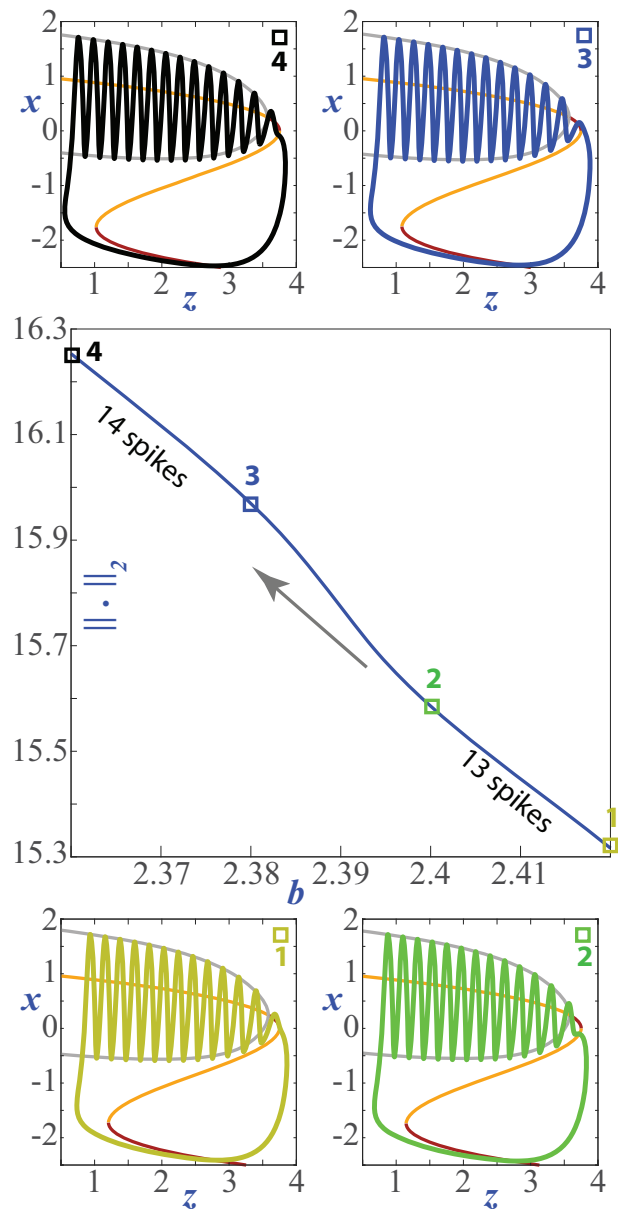


FIG. 7. Evolution of periodic orbits throughout the process of Hopf-induced continuous spike-adding. Central picture shows the bifurcation diagram obtained by continuation corresponding to the segment $R1b$ of Fig. 2. The coloured squares mark the points in the diagram corresponding to the selected values. The stable periodic orbits are shown over the slow \mathcal{M}_{slow} and fast \mathcal{M}_{fast} manifolds. The grey arrow indicates the direction in the process of adding a new spike. Along the continuation of the bifurcation line we observe how periodic orbits with thirteen spikes move to the left so that space is generated for the appearance of a new spike on the right side of the orbit. Finally, periodic orbits have fourteen spikes.

ation software stops the calculation of the fold bifurcations. We show an intermediate segment ($R3b$) where the passage through the canard is not so apparent.

In order to illustrate more clearly the transition between these two types of spike-adding, we study one case for a

This is the author's peer reviewed, accepted manuscript. However, the online version of record will be different from this version once it has been copyedited and typeset.
PLEASE CITE THIS ARTICLE AS DOI: 10.1063/5.0037942

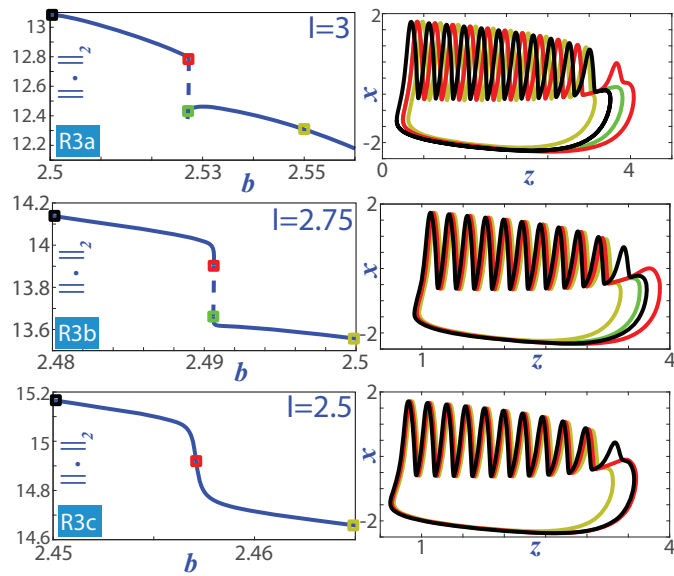


FIG. 8. Variations of the spike-adding processes along segments $R3a$, $R3b$ and $R3c$ (Fig. 2). Along segment $R3a$ (top) the spike-adding is canard-induced, but along segment $R3c$ (bottom) the bifurcation curve has been stretched and the spike-adding process is Hopf-induced.

407 higher value of the small parameter ($\varepsilon = 0.05$) to help in
 408 the visualization. For this ε value, the two fold bifurca-
 409 tions involved in the spike-adding from 2 to 3 spikes between
 410 fold/hom bursters that occur in the upper part of the region be-
 411 low the homoclinics can be fully continued numerically. Fold
 412 bifurcation curves are plotted in yellow in Fig. 9. They arise
 413 from codimension-two bifurcation points located on the ho-
 414 moclinic curves. Segments A and B cut both curves and, as it
 415 can be seen on the bottom pictures, the spike-adding process
 416 is canard-induced. If we compare the continuation bifurca-
 417 tion curves (left pictures) for both segments, we can observe
 418 how, as l decreases, the curve is stretched. As a consequence,
 419 the two fold bifurcation curves get closer to each other, un-
 420 til they reach a point (cusp bifurcation) where both coincide
 421 and disappear. Segment C goes through that point. This is
 422 the bifurcation point where canard-induced continuous spike-
 423 adding ends to give rise to Hopf-induced continuous spike-
 424 adding. Segments D and E cross this type of spike-adding, as
 425 can be seen on bottom pictures.

426 Once we understand how a cusp bifurcation of periodic or-
 427 bits allows us to explain the passage from a canard-induced
 428 spike-adding towards a Hopf-induced type, we can conjecture
 429 that this is what happens for smaller values of ε and, in particu-
 430 lar, in the case illustrated in Fig. 8, although the fold bifurca-
 431 tion curves involved are not easy to detect and to continue. It
 432 is important to remark here one main difference among both
 433 continuous spike-adding phenomena: in the canard-induced
 434 case the canard orbit in the process to obtain an extra spike
 435 makes a “go-and-come-back” excursion, whereas in the Hopf-
 436 induced case the orbit that is obtaining an extra spike grows
 437 but it does not come back. This is clearly seen in Figures 8

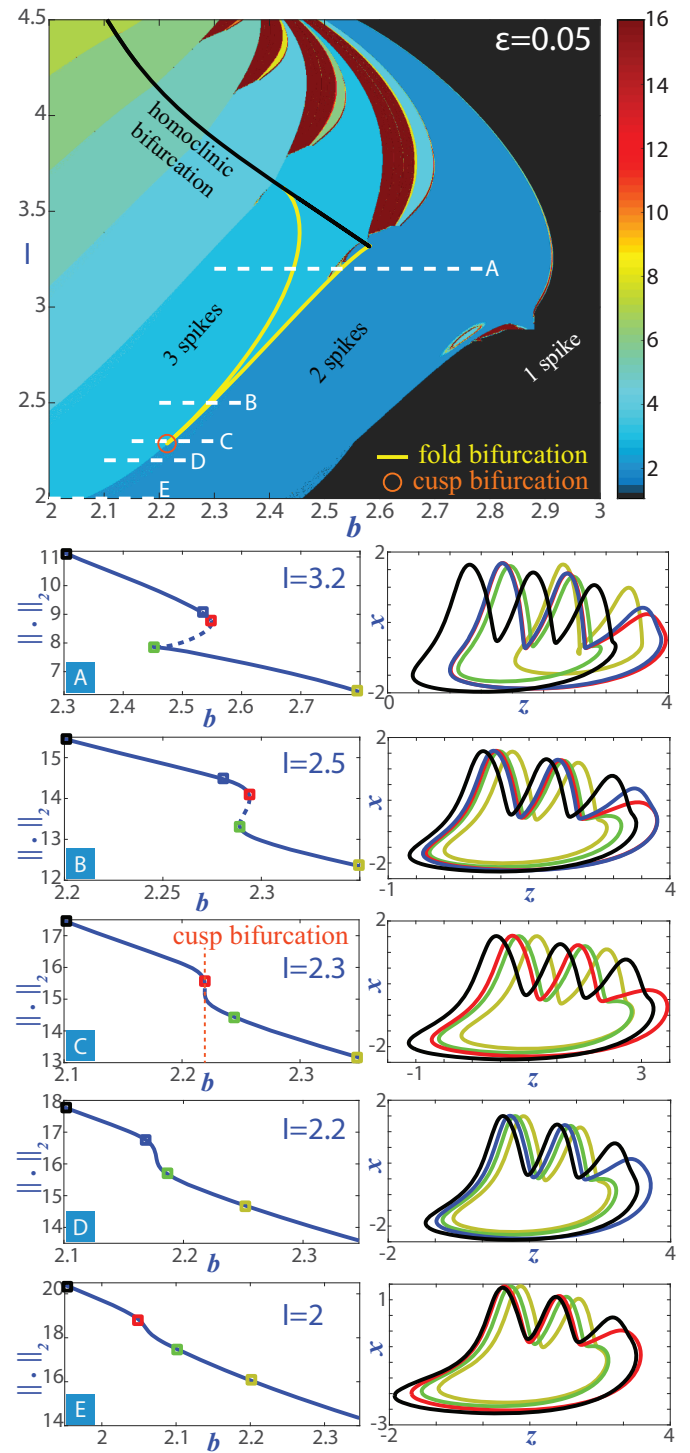


FIG. 9. Top: Biparametric bifurcation spike-counting diagram for $\varepsilon = 0.05$. Different segments are selected to illustrate the evolution from canard-induced continuous spike-adding (segments A and B) to Hopf-induced continuous spike-adding (segments D and E) through a cusp (segment C). Bottom: Left column shows bifurcation diagrams obtained by continuation corresponding to the selected segments. In the right column, some periodic orbits along the segment are plotted together to see their relative position and shape. The colors of the orbits correspond with coloured squares in the left bifurcation diagrams.

438 and 9.

439 As already mentioned, the transition from the region where
440 spike-adding is induced by chaotic dynamics to the zones ex-
441 hibiting continuous processes is determined, one way or an-
442 other, by the homoclinic skeleton of the model. Two cases
443 are clearly distinguished according to whether the dynamics
444 change to either a canard-mediated mechanism or a Hopf-
445 induced one.

446 If we pay attention to the transition towards a canard-
447 induced spike-adding, the homoclinic bifurcation curve it-
448 self becomes a sharp frontier with the region governed by
449 the chaotic machinery. Indeed, if we consider any horizon-
450 tal line in the parameter space such that it crosses the homo-
451 clinic curve, as the long segment $R1$ in discontinuous orange
452 in Fig. 2, the passage through the homoclinic curve is clearly
453 the event which marks the change of behavior. As illustrated
454 in Fig. 12, which is included in the Discussion section, the
455 spike-adding transition from 2 to 3 spikes consists of a chaotic
456 window (see Section II A), whereas in the passage from 3 to
457 4 spikes a bistability window is traversed (see Section II B).
458 In between, the homoclinic curve is crossed, and large chaotic
459 windows are no longer observed to the left of such bifurcation.

460 The transformation of discontinuous spike-addings into
461 Hopf-induced ones is quite different. To describe how dynam-
462 ics evolve, we have selected a short segment in the parameter
463 space fixing $I = 4.1$ and $b \in [2.58, 2.6]$. We denote by $P1$ and
464 $P2$ the left and right ends, respectively (see Fig. 2). The
465 transition process starts when the segment crosses an ultimate fan
466 of bifurcation curves of periodic orbits arising from the type-
467 C inclination-flip (IF) codimension-two homoclinic bifurca-
468 tion point located in the fold of the homoclinic curve (see the
469 theoretical unfolding³⁴ and the numerically computed bifurca-
470 tion curves displayed at the bottom-right panel in Fig. 10).
471 As showed at top panels of Fig. 10, for $P1$ and $P2$ we observe
472 a fold/Hopf and a fold/hom bursting, respectively. Some of
473 the changes that occur in the attractor can be seen in the IBD
474 bifurcation diagram (central panel of Fig. 10). By decreasing
475 parameter b , a bistability zone is detected, which leads to the
476 gaining of a new spike. It is formed as a consequence of the
477 passing through fold and period-doubling bifurcation curves.
478 Shortly after crossing this bistability zone, there is an abrupt
479 change in the number of spikes that precedes the entrance into
480 the domain of Hopf-induced spike-adding (see the green verti-
481 cal band in the IBD). The time series and the orbit exhibited
482 at the bottom-left panel in Fig. 10 show a phenomenon of in-
483 termittency where the fold/Hopf and the fold/Hom bursting al-
484 ternate (the sum of the spikes of both types explains the abrupt
485 jump observed in the IBD). We can understand this peculiar
486 behavior appealing to the fast-slow decomposition. Along the
487 transition from fold/Hopf to fold/hom bursting (see Fig. 1),
488 the 2D fast manifold of limit cycles becomes tangent to the
489 1D slow manifold of equilibria. Close to this tangency, orbits⁴⁹⁶
490 can show the alternation between the two types of bursting,
491 exhibiting phases where the orbit follows the fast manifold up⁴⁹⁷
492 to the Hopf bifurcation point and phases where orbits behave⁴⁹⁸
493 as if the fast manifold were split. The presence of the pen-⁴⁹⁹
494 cils of bifurcations that converge to the IF point helps in this⁵⁰⁰
495 mixed behavior. 501

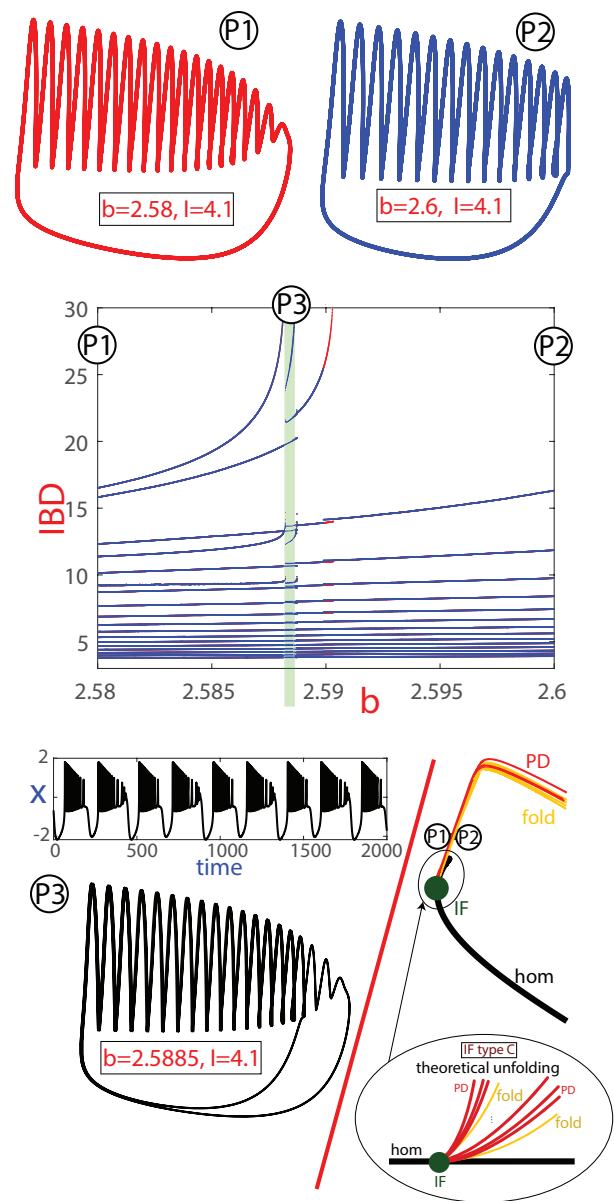


FIG. 10. Crossing the bridge between Hopf-induced (top-left) and chaos-induced (top-right) spike-adding. Orbits correspond to points $P1$ and $P2$, respectively, of Fig. 2. Inter-spikes bifurcation diagram for $I = 4.1$ and $b \in [2.58, 2.6]$ is provided in central panel, where the green vertical band separates the two types of spike-adding. Transition through the green band is illustrated at the bottom-left panel. Bottom-right panel provides the location of $P1$ and $P2$, and also the numerically calculated bifurcation curves and the theoretical unfolding of a type-C inclination-flip.

IV. DISCUSSION

Throughout the previous sections we have provided a unified perspective of several of the spike-adding mechanisms that are unfolded in the Hindmarsh-Rose model and the transitions that occur between the different types. Figure 11 provides a schematic illustration of the catalogue. Specifically,

502 we have identified:

- 503 • **Chaos-induced spike-adding:** (translucent red region)
504 discontinuous spike-adding formed by isolas of burst-
505 ing periodic orbits with cascades of period-doubling bi-
506 furcations leading to chaos. This case corresponds to
507 the chaotic scenario studied by Terman²³.
 - 508 • **Canard-induced continuous spike-adding:** (translu-
509 cent dark-blue region) continuous spike-adding created
510 in hysteresis areas limited by fold bifurcations of peri-
511 odic orbits and canards being involved in the genesis of
512 extra spikes.
 - 513 • **Hopf-induced continuous spike-adding:** (translucent
514 pale-green region) continuous spike-adding with a Hopf
515 bifurcation being involved in the creation of new extra
516 spikes (see also Appendix).
 - 517 • **Transition spike-adding states:** there are three possi-
518 bilities. Translucent green strips shown in Fig. 11
519 correspond to the transition between Hopf-induced and
520 canard-induced continuous spike-addings near a cusp
521 bifurcation where two fold bifurcations of periodic ori-
522 bits collapse. Sharp location is not possible because,
523 as already explained in Section III, the cusp points
524 are not easy to detect and, furthermore, they do not
525 form a continuous line as they appear just at isolated
526 points (they are codimension-two bifurcations). On the
527 contrary, the frontier in between chaos-induced spike
528 adding and the other two mechanisms is evident. The
529 black curve (homoclinic bifurcation) marks the transi-
530 tion to canard-induced spike-adding. The change from
531 chaos- to Hopf-induced spike-adding involves bifurca-
532 tion curves of periodic orbits arising from codimension-
533 two homoclinic bifurcations and it is clearly recogniz-
534 able on the spike-counting bifurcation diagram.
- 535 Just as a summary of what is typically observed in numer-
536 ical and experimental settings, Figure 12 shows a one param-
537 eter slice (line $R1$ in Fig. 2) where the three types of spike-
538 adding detected in the model (chaos-induced discontinuous
539 spike-adding (right), canard-induced continuous spike-adding
540 (middle) and Hopf-induced continuous spike-adding (left))
541 and two transitions in between are observed. In the plot
542 at the top (a), the interspike-interval bifurcation diagram (IBD)
543 shows clearly the number of spikes and the time length among
544 spikes. Red color represents coexistence of two periodic at-
545 tractors with n and $n + 1$ spikes. The bottom plot (b) presents
546 the parametric evolution of the periodic orbits using contin-
547 uation techniques. The figure shows the $\|\cdot\|_2$ norm of the
548 periodic orbit along the selected segment $R1$. In the contin-
549 uation line, the blue color line changes from Hopf-induced
550 continuous spike-adding (left part) to canard-induced contin-
551 uous spike-adding (middle part). Note that, on the right side
552 the purple color line represents an isola (simple closed curves
553 in the corresponding slice) of 3-spikes periodic orbits
554 and green and other colors represent the basic 2-spikes periodic or-
555 bit and its period-doubling bifurcated orbits on the region of

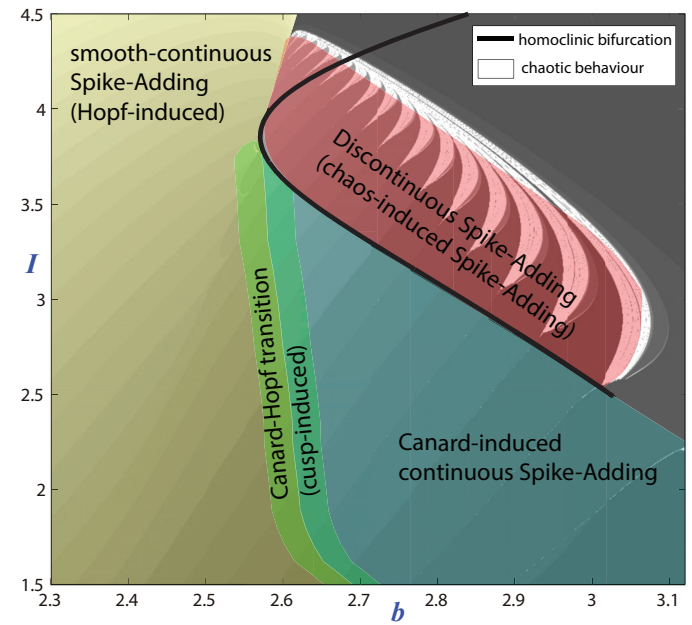


FIG. 11. Classification scheme of regions with different type of spike-adding process superimposed on the biparametric bifurcation spike-counting diagram for $\varepsilon = 0.01$. White color represents regions with chaotic behavior; different shades of gray represent regions with periodic orbits with different number of spikes; translucent colors represent (schematically) regions with different types of spike-adding. The homoclinic bifurcation (black curve) marks the boundary between the region with discontinuous spike-adding and the other regions.

chaos-induced discontinuous spike-adding. We can also observe how the change from the discontinuous spike-adding to the continuous spike-adding occurs sharply when crossing the homoclinic curve. On the other hand, while canard-induced continuous spike-adding is occurring, the segment $R1$ crosses bistability wedges, limited by a fold point and the first period-doubling bifurcation. When the last wedge has been crossed, the spike-adding mechanism changes to Hopf-induced. Note that bistability regions are only present in the canard-induced continuous spike-adding.

Fig. 12 also shows the vertical line ($b = 2.67434$) that, according to the fast-slow dynamics and the Izhikevich classification, corresponds to the passage from fold/hom to fold/Hopf bursting. Namely, in the biparametric plane (b, I), the vertical line $b = 2.67434$ is tangent to the homoclinic bifurcation curve for the fast subsystem at the point where the curve folds in the b -direction. Of course, since this useful classification is based on the limit case ($\varepsilon = 0$), this theoretical frontier works the better as smaller the value of ε is and, in fact, already for $\varepsilon = 0.01$ we observe how the Izhikevich criterion is no longer applicable in some regions.

Indeed, paying attention to the cascade of bifurcations shown at panel (b) of Fig. 12, it is still observed how on the left side of the vertical line of homoclinic folding, the canards are involved in the genesis of new spikes. On this side, the Izhikevich analysis classifies the bursting as fold/Hopf, but this only

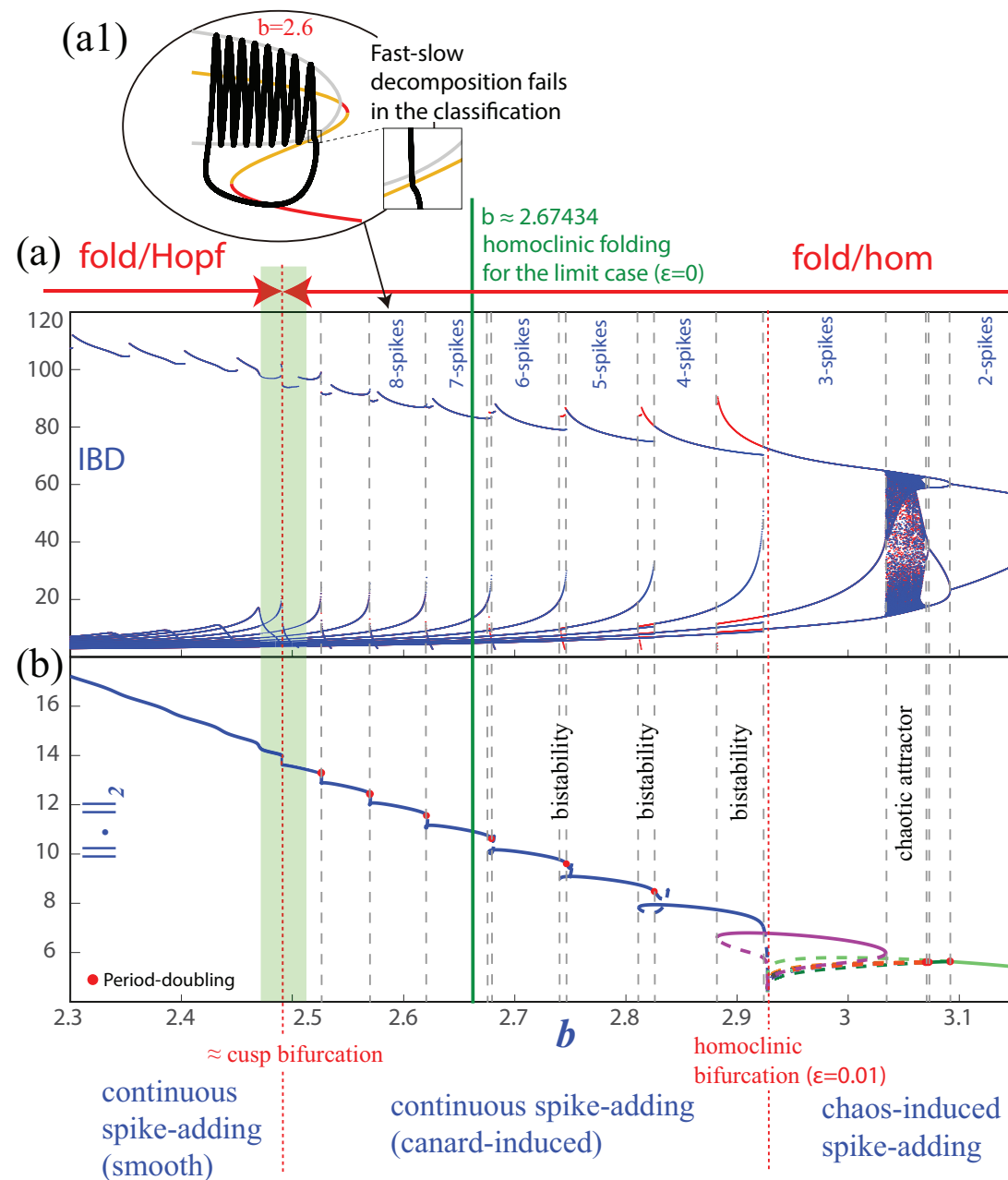


FIG. 12. Analysis of transitions along segment $R1$ (in Fig. 2) with $\varepsilon = 0.01$, $I = 2.75$ and b as bifurcation parameter. (a) Interspike-interval bifurcation diagram (IBD). Red color represents coexistence of two periodic attractors with n and $n + 1$ spikes. Panel (b) shows the $\|\cdot\|_2$ norm of the periodic orbit along the process, obtained with continuation techniques (AUTO). Purple represents an isola of 3-spikes periodic orbits; the continuous spike-adding process is shown in blue; green and other colors represent the basic 2-spikes periodic orbit and its period-doubling bifurcated orbits. More details are given in the text. Panel (a1) illustrates one example of the limits with Izhikevich's classification.

582 manifests for smaller values of parameter b (on the left-side) 591
 583 of the cusp bifurcation line, to be precise). The reason lies 592
 584 in the fact that for a higher dimensional parameter space, like 593
 585 in a three-dimensional bifurcation diagram including ε , the 594
 586 transition bifurcation surfaces exhibit some inclination, that is, 595
 587 they are not completely vertical (see recent Ref. 10 for a complete 596
 588 three dimensional analysis). Panel (a1) in Fig. 12 illus- 597
 589 trates with an example the limitations with Izhikevich's clas- 598
 590 sification. Superimposed on the fast-slow decomposition, a 599

bursting orbit is shown. Fast-slow decomposition is fold/Hopf type, but bursting is clearly of fold/hom type.

From a practical point of view, we may have the following question: how does this study help in biological settings? In fact, the main point is to consider what phenomena we can expect. Obviously, it is not possible to determine the spike-adding mechanisms that a neuron experiences only with experimental data. Nevertheless, the visualization of a bursting orbit and the information obtained from biparametric maps

This is the author's peer reviewed, accepted manuscript. However, the online version of record will be different from this version once it has been copyedited and typeset.
PLEASE CITE THIS ARTICLE AS DOI: 10.1063/1.50037942

600 arising in simpler models can help us to point to one type or 655
601 another. That is, if a square-wave bursting solution (fold/hom 656
602 case) is observed, we should have in mind two possible spike 657
603 adding mechanisms: canard-induced or chaos-induced. If ex 658
604 perimentation shows abrupt changes in the number of spikes, 659
605 we can suspect that there is a hysteresis phenomenon and 660
606 that the dynamics have been captured by an alternative sta 661
607 ble branch, so we identify a canard-induced spike-adding 662
608 The recognition of this mechanism should move researche 663
609 to look for the coexisting stable orbit since bistability is, in 664
610 many cases, a desirable feature of a neuron and may have bi 665
611 ological consequences^{35–37}. On the contrary, if some chaotic 666
612 phenomenon is detected, we can suspect the existence of iso 667
613 las and that the spike-adding processes may involve transi 668
614 tions through chaotic windows³⁸. Furthermore, there are ex 669
615 amples in the literature of experiments with neurons exhibit 670
616 ing comb-shaped biparametric structures associate to chaos 671
617 induced mechanisms^{39–41}. In these examples, the use of bi 672
618 parametric maps helps to explain the results. The appearance 673
619 of fold/Hopf bursting orbits is the signal that either bistabil 674
620 ity or chaos are over and the spike-adding becomes a smooth
621 process. The above ones are not the only precursors of the
622 different phenomena. For example, a bursting orbit that sud 675
623 denly lengthens and then returns, but with an extra spike, can
624 be identified with the presence of a canard phenomenon and
625 bistability. 676

626 From a mathematical point of view, once the global struc 677
627 ture is clear, one can think of obtaining analytical proofs to ex 678
628 plain how the different processes and transformations emerge 679
629 from the singular limit using, for instance, the techniques in 680
630 troduced by P. Carter^{25,27}. We also remark that, taking into 681
631 account that the codimension-two points are organizing cen 682
632 ters for key bifurcations involved in some of the processes
633 and transitions analysed in this paper, it should be interesting
634 to study the existence of codimension-three points unfolding 684
635 these codimension-two bifurcations, but we have to move into
636 a three-parametric space, like in Ref. 10, and this is part of our
637 future research. 685

638 V. CONCLUSIONS 688

639 Neural communication takes place through action poten 689
640 tials or spikes. In addition, it is when the spikes travel in 690
641 packets that the exchange of information is more fluent and 691
642 efficient. The number and tempo of the spikes in each burst 692
643 are main ingredients to build neural messages. These are 693
644 the reasons that justify the importance of the analysis of the 694
645 spike-adding mechanisms. In this paper we deal with bursting 695
646 in single-neurons activity. Among the most popular models, 696
647 we choose the Hindmarsh-Rose, as it is the simplest one that 697
648 is able to exhibit bursting behavior. We show and classify 698
649 the different mechanisms of spike-adding: chaos-induced, 699
650 canard-induced and Hopf-induced. Besides, we study the 700
651 transition mechanisms from one type of spike-adding process 701
652 to another. 702

653 The above processes involve bistable and chaotic regimes, 703
654 As already mentioned, bistability is a profitable character 704

istic for a neuron and chaotic behaviors are commonly ob 705
655 served in experiments with real neurons in the laboratory, as
656 in Refs. 38–41. Our theoretical results motivate the interest
657 for discovering new mechanisms in the context of the cited
658 experiments. 706

Spike-adding maps provide us with information on how we
659 should move in the parameter space depending on whether we
660 want our neuron to exhibit one or another spike-adding mech 707
661 anism. These maps are common in the literature and simi 708
662 lar chaotic zones and spike-adding stripes have been found
663 for other realistic fold/hom bursting models, including the
664 leech heart interneuron model⁴² and the pancreatic β -cell neu 709
665 ron model⁴³, among others. Therefore, for future research,
666 it would be interesting to explore whether this classification
667 is valid in other models exhibiting fold/hom and fold/Hopf
668 bursting, where we sincerely believe that this is the case. And
669 what is more challenging, Izhikevich's catalogue for the types
670 of bursting is extensive and one must wonder what spike-
671 adding mechanisms are available in each case and also what
672 are the transition dynamics. 709

ACKNOWLEDGMENTS

RB and SS have been supported by the Spanish Research
673 projects PGC2018-096026-B-I00 and PID2019-105674RB-
674 I00, the Universidad de Zaragoza-CUD project UZCUD2019-
675 CIE-04 and the European Regional Development Fund and
676 Diputación General de Aragón (E24-17R and LMP124-18).
677 SI and LP have been supported by Spanish Research project
678 MTM2017-87697-P. LP has been partially supported by the
679 Gobierno de Asturias project PA-18-PF-BP17-072.

DATA AVAILABILITY

Data available on request from the authors. The simula 710
685 tions have been done using the AUTO^{29,30} and TIDES^{44,45}
686 softwares. 711

- 688 ¹F. Zeldenrust, W. J. Wadman, and B. Englitz, *Frontiers in Computational*
689 *Neuroscience* **12**, 48 (2018).
- 690 ²R. Barrio and A. Shilnikov, *Journal of Mathematical Neuroscience* **1**, 6:1
691 (2011).
- 692 ³J. G. Freire and J. A. C. Gallas, *Phys. Chem. Chem. Phys.* **13**, 12191 (2011).
- 693 ⁴X.-B. Rao, Y.-D. Chu, Lu-Xu, Y.-X. Chang, and J.-G. Zhang, *Communica-*
694 *tions in Nonlinear Science and Numerical Simulation* **50**, 330 (2017).
- 695 ⁵B. Jia, *Chinese Physics B* **23**, 030505 (2014).
- 696 ⁶J. L. Hindmarsh and R. M. Rose, *Proc. Roy. Soc. Lond.* **B221**, 87 (1984).
- 697 ⁷J. Rinzel, in *Mathematical Topics in Population Biology, Morphogenesis*
698 *and Neurosciences: Proceedings of an International Symposium held in*
699 *Kyoto, November 10–15, 1985*, edited by E. Teramoto and M. Yumaguti
700 (Springer Berlin Heidelberg, Berlin, Heidelberg, 1987) pp. 267–281.
- 701 ⁸E. M. Izhikevich, *Int. J. Bifur. Chaos Appl. Sci.* **10**, 1171 (2000).
- 702 ⁹R. Barrio, S. Ibáñez, and L. Pérez, *Phys. Lett. A* **381**, 597 (2017).
- 703 ¹⁰R. Barrio, S. Ibáñez, and L. Pérez, *Chaos* **30**, 053132, 20 (2020).
- 704 ¹¹R. Barrio, S. Ibáñez, L. Pérez, and S. Serrano, *Commun. Nonlinear Sci.*
705 *Numer. Simul.* **83**, 105100, 15 (2020).
- 706 ¹²R. Barrio, M. A. Martínez, S. Serrano, and A. Shilnikov, *Chaos* **24**, 023128
707 (2014).
- 708 ¹³M. Desroches, T. J. Kaper, and M. Krupa, *Chaos* **23**, 046106 (2013).
- 709 ¹⁴J. M. González-Miranda, *Chaos* **13**, 845 (2003).

- 710 ¹⁵J. M. González-Miranda, *Physical Review E* **72**, 051922 (2005). 771
 711 ¹⁶J. M. Gonzalez-Miranda, *Int. J. Bifur. Chaos Appl. Sci.* **17**, 3071 (2007). 772
 712 ¹⁷G. Innocenti, A. Morelli, R. Genesio, and A. Torcini, *Chaos* **17**, 043128 773
 713 (2007).
 714 ¹⁸G. Innocenti and R. Genesio, *Chaos* **19**, 023124 (2009). 774
 715 ¹⁹D. Linaro, A. Champneys, M. Desroches, and M. Storace, *SIAM J. Appl.*
 716 *Dyn. Syst.* **11**(3), 939–962 (2012).
 717 ²⁰M. Storace, D. Linaro, and E. de Lange, *Chaos* **18**, 033128 (2008).
 718 ²¹A. Shilnikov and M. Kolomiets, *Int. J. Bifur. Chaos Appl. Sci.* **18**(8), 2141
 719 (2008).
 720 ²²N. Fenichel, *J. Differential Equations* **31**, 53 (1979).
 721 ²³D. Terman, *SIAM J. Appl. Math.* **51**, 1418 (1991). 775
 722 ²⁴J. Nowacki, H. M. Osinga, and K. Tsaneva-Atanasova, *The Journal of*
 723 *Mathematical Neuroscience* **2**, 7 (2012).
 724 ²⁵P. Carter, *Journal of Nonlinear Science* **30**, 1432 (2020).
 725 ²⁶C. Morris and H. Lecar, *Biophys. J.* **35**, 193 (1981).
 726 ²⁷P. Carter and B. Sandstede, *SIAM Journal on Applied Dynamical Systems* **17**, 236 (2018). 776
 727 ²⁸Y. A. Kuznetsov, *Elements of applied bifurcation theory*, 3rd ed., Applied
 728 *Mathematical Sciences*, Vol. 112 (Springer-Verlag, New York, 2004) pp.
 729 xxii+631.
 730 ²⁹E. Doedel, in *Proceedings of the Tenth Manitoba Conference on Numerical*
 731 *Mathematics and Computing, Vol. 1 (Winnipeg, Man., 1980)*, Vol. 30 (1981) 777
 732 pp. 265–284.
 733 ³⁰E. J. Doedel, R. Paffenroth, A. R. Champneys, T. F. Fairgrieve,
 734 Y. A. Kuznetsov, B. E. Oldeman, B. Sandstede, and X. J. Wang,
 735 <http://cmv1.cs.concordia.ca/auto>.
 736 ³¹Y. Pomeau and P. Manneville, *Comm. Math. Phys.* **74**, 189 (1980). 779
 737 ³²E. Ott, *Chaos in dynamical systems*, 2nd ed. (Cambridge University Press,
 738 Cambridge, 2002) pp. xii+478.
 739 ³³X. Wang, *Physica D* **62**, 263 (1993).
 740 ³⁴A. J. Homburg and B. Sandstede, *Handbook of Dynamical Systems* **3**, 379 780
 741 (2010).
 742 ³⁵A. Dovzhenok and A. S. Kuznetsov, *PLOS ONE* **7**, 1 (2012).
 743 ³⁶W. Barnett, G. O'Brien, and G. Cymbalyuk, *Journal of Neuroscience Meth-*
 744 *ods* **220**, 179 (2013).
 745 ³⁷M. Uzuntarla, *Neurocomputing* **367**, 328 (2019).
 746 ³⁸H. Gu, *Chaos* **23**, 023126 (2013).
 747 ³⁹W. Xiao-Bo, M. Juan, Y. Ming-Hao, Z. Qiao-Hua, G. Hua-Guang, and
 748 R. Wei, *Chinese Physics Letters* **25**, 2799 (2008).
 749 ⁴⁰H. Gu, *PLOS ONE* **8**, 1 (2013).
 750 ⁴¹H. Gu, B. Pan, G. Chen, and L. Duan, *Biological Cybernetics* **78**, 391
 751 (2014).
 752 ⁴²R. Barrio, M. Lefranc, M. A. Martínez, and S. Serrano, *EPL (Europhysics*
 753 *Letters)* **109**, 20002 (2015).
 754 ⁴³E. Mosekilde, B. Lading, S. Yanchuk, and Y. Maistrenko, *BioSystems* **63**,
 755 3 (2001).
 756 ⁴⁴A. Abad, R. Barrio, F. Blesa, and M. Rodríguez, 781
 757 <https://sourceforge.net/projects/tidesodes/>. 782
 758 ⁴⁵A. Abad, R. Barrio, F. Blesa, and M. Rodríguez, *ACM Transactions on* 783
 759 *Mathematical Software* **39**, 5:1 (2012). 784
 760

761 APPENDIX

762 In this Appendix we just show analytically, with a simple
 763 example, how an increase in the distance between the saddle- 787
 764 node bifurcations of equilibria in the fast subsystem of the HR
 765 model allows the increment of the number of spikes, and so,
 766 it generates the Hopf-induced spike-adding process.

767 Let us consider the following family of vector fields:

$$788 \begin{cases} x' = -zx - \omega y - Lx(x^2 + y^2), \\ y' = \omega x - zy - Ly(x^2 + y^2), \\ z' = \varepsilon. \end{cases} \quad (A.1) \quad 790$$

789 This is a toy-model for a Hopf bifurcation, where the bifurca- 792
 793 tion parameter z varies with respect to time at a constant ratio 794
 795 ε , which we assume to be a small parameter ($\varepsilon \ll 1$). Coeffi-

cient L corresponds to the first Lyapunov coefficient²⁸ and we
 assume that $L > 0$.

Using polar coordinates $x = r \cos \theta$, $y = r \sin \theta$ in (A.1), we
 get:

$$\begin{cases} r' = -zr - Lr^3, \\ \theta' = \omega, \\ z' = \varepsilon. \end{cases} \quad (A.2)$$

Let

$$\varphi(t, r_0, \theta_0, z_0) = (\varphi^r(t, r_0, \theta_0, z_0), \varphi^\theta(t, r_0, \theta_0, z_0), \varphi^z(t, r_0, \theta_0, z_0))$$

be the flow defined by equations (A.2). Clearly,

$$\begin{aligned} \varphi^\theta(t, r_0, \theta_0, z_0) &= \theta_0 + \omega t, \\ \varphi^z(t, r_0, \theta_0, z_0) &= z_0 + \varepsilon t. \end{aligned}$$

Fixing time $t = \frac{2\pi}{\omega}$ and angle $\theta_0 = 0$ we get the first return
 map P from the half-plane $\theta_0 = 0$ on itself. Namely,

$$P(r_0, z_0) = (P^r(r_0, z_0), P^z(r_0, z_0))$$

with

$$P^r(r_0, z_0) = \varphi^r\left(\frac{2\pi}{\omega}, r_0, 0, z_0\right)$$

and

$$P^z(r_0, z_0) = \varphi^z\left(\frac{2\pi}{\omega}, r_0, 0, z_0\right) = z_0 + \frac{2\pi\varepsilon}{\omega}.$$

In what follows, we assume that

$$(r_0, z_0) \in [0, R] \times \{-\delta\},$$

for some $\delta > 0$ and $R > \sqrt{\frac{\delta}{L}}$, and define

$$(r_n, z_n) = ((P^r)^n(r_0, z_0), (P^z)^n(r_0, z_0)).$$

Constant δ stands for the maximum allowed change in pa-
 rameter z . We say that the orbit of the point $(r_0, 0, z_0)$ has N
 spikes if N is the maximum number of iterations of the first re-
 turn map which remain in the rectangle $[0, R] \times [-\delta, \delta]$. Since
 785 $R > \sqrt{\frac{\delta}{L}}$, it follows by construction that $r_n < R$ for all $n \in \mathbb{N}$.
 786 On the other hand

$$z_n = -\delta + \frac{2\pi\varepsilon n}{\omega},$$

and, in order to have $z_n > \delta$, the condition

$$n > \frac{\delta\omega}{\pi\varepsilon},$$

788 must be fulfilled. We obtain the expected results, that is, the
 789 number n of allowed spikes increases as either δ or the rota-
 790 tion speed ω increase. Bearing in mind the Hindmarsh-Rose
 791 model, the number of spikes in the fold/Hopf bursting in-
 792 creases as the distance (measured in the z -direction) between
 793 the two saddle-node bifurcation points in the fast subsystem
 (2 δ in the toy model) increases.